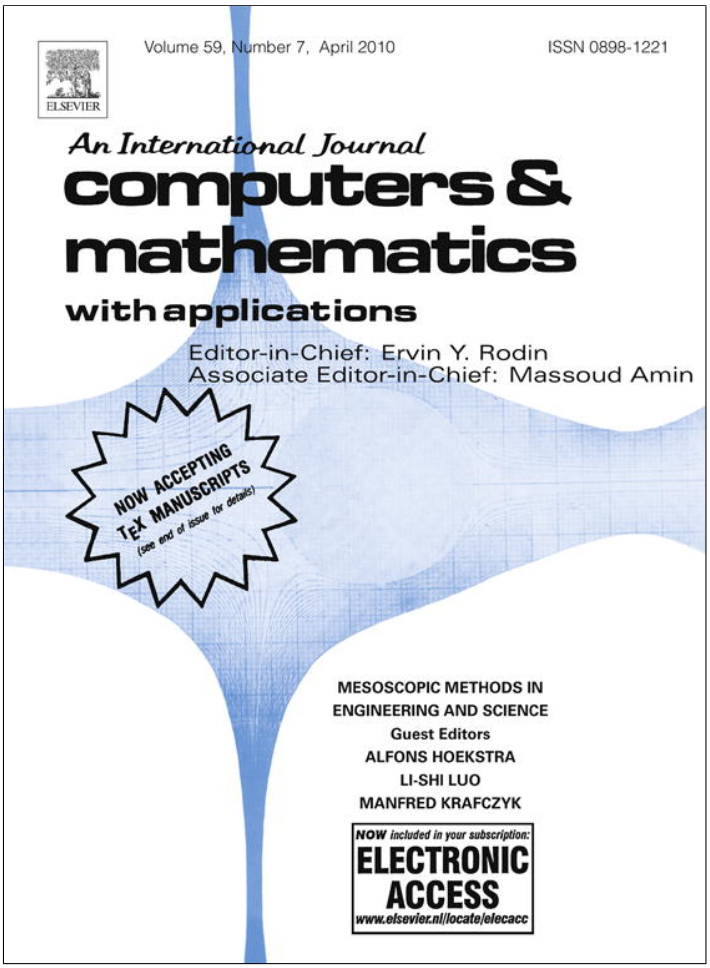

Computers and Mathematics with Applications 59 (2010) 2260–2270

Contents lists available at ScienceDirect

Computers and Mathematics with Applications

journal homepage: www.elsevier.com/locate/camwa

# Multirange multi-relaxation time Shan–Chen model with extended equilibrium

A. Kuzmin *, A.A. Mohamad

*Department of Mechanical and Manufacturing Engineering, Schulich School of Engineering, University of Calgary, 2500 University Drive NW, Calgary, T2N 1N4 Canada*

ARTICLE INFO

*Keywords:*
Multiphase flow
Shan–Chen model
Surface tension
Multirange potential
Gas–liquid density ratio
Multi-relaxation time

ABSTRACT

The work presents simulations with the multirange Shan–Chen model developed by Sbragaglia et al. (2007) [18], which improved the Shan–Chen model for the proper surface tension term. Also, by introducing the matrix collision operator and extended equilibrium density distribution function, the density ratio is increased from 100 to 160. The Multi-Relaxation Time (MRT) method attracted the attention of researchers due to several advantages, such as better stability, simulations with Prandtl number different from unity, and possibilities to improve the accuracy of the scheme compared with BGK Single Time Relaxation model. Our recent results have shown that the combination of MRT methods with multiphase flow models can improve the achievable gas–liquid density ratio.



## 1. Introduction

Lattice Boltzmann Method (LBM) has emerged as a powerful competitor for conventional Computational Fluid Dynamics (CFD) methods, especially for simulations of multiphase flows and flows with complex boundary conditions. Recent review about curved boundaries, grid-refinement, force evaluation, and boundary conditions is given by [1]. General reviews and introduction to the LBM can be found in the books [2–4].

There are several approaches to model multiphase behavior. Based on the cellular automata color model of Rothman et al. [5], Gunstensen et al. [6] proposed a lattice Boltzmann color scheme able to imitate multiphase behavior. Later on, He et al. [7] used a series expansion of intermolecular potential to obtain a proper force term accounting for multiphase behavior. Two sets of distribution functions were used for tracking phase interface, pressure and velocity fields. Swift et al. [8] developed a model for non-ideal fluids to account for the interfacial thermodynamics, utilizing the free energy approach. Luo [9] and Lee and Lin [10] introduced finite density and pressure-based multiphase models, respectively. The most popular model, to the best of the authors' knowledge, is the model of Shan and Chen [11] utilizing the pseudo-potential for intermolecular potential.

There is no model without drawbacks. For instance, the original Gunstensen model needs extensive computer resources [2], and the He model [7] suffers from numerical instabilities associated with the "stiffness" of the collision operator, and the Swift model [12] lacks the Galilean invariance. To address these difficulties many researchers significantly improved the mentioned models. Ahrenholz et al. [13], Ginzburg and Steiner [14], and Kehrwald [15] reformulated the Gunstensen scheme. Level set coupling by Thömmes et al. [16] gave better performance, and further improvements of Galilean invariance were presented in Yeomans [17]. The numerical instabilities of the Rothman–Gunstensen model and the Shan–Chen model are thought to be respectively connected to the different sound speeds in both media [15], and to the spurious currents.

* Corresponding author.
*E-mail addresses:* shurik.kuzmin@gmail.com (A. Kuzmin), mohamad@ucalgary.ca (A.A. Mohamad).

0898-1221/$ – see front matter © 2009 Elsevier Ltd. All rights reserved.
doi:10.1016/j.camwa.2009.08.042

The present work concentrates on the Shan–Chen multiphase model. Shan and Chen [11] (SC) proposed a multiphase model where forces are directly encoded as the result of pairwise molecular interactions (pseudo-potential). In the model, an additional momentum forcing term is explicitly added to the velocity field at each time step. The model is popular because it is conceptually straightforward. However, the model is not consistent with thermodynamic behavior [8] and can only handle moderate liquid–vapor density ratios [18]. Also, the model cannot control the gas–liquid ratio and surface tension term separately [19]. The surface tension term in the Shan–Chen model has a different form from the Navier–Stokes surface tension term and depends on the pseudo-potential [18].

The objective of this research is to improve the Shan–Chen model by (1) achieving better gas–liquid densities, (2) controlling gas–liquid ratio and interface width separately. This can be achieved by using the Multi-Relaxation Time (MRT) collision operator along with the multirange Shan–Chen potential [18]. Proper choice of parameters for the multirange Shan–Chen model allows the elimination of the non-Navier–Stokes surface tension term and it's dependency on the same parameter $G_1$ in the equation of state. Thus, the interface width and gas–liquid ratio can be controlled by different parameters. Moreover, the surface tension term is consistent with the Navier–Stokes equation. In addition, this work presents the extended equilibrium distribution function, which comes along with extended lattice Boltzmann models beyond the Navier–Stokes equation [20]. The combination of these approaches facilitates the doubling of the gas–liquid ratio. The work presented is an extension of our previous work [21] with the multirange potential and the extended equilibrium distribution function.

The inability for the Shan–Chen model to achieve high gas–liquid densities are due to spurious currents [2]. Those come from higher-order anisotropy in the Shan–Chen force term [22,18], causing high Mach numbers to destroy the stability of the multiphase scheme. Spurious currents can be treated by applying a better numerical approximation for the Shan–Chen force. This involves a larger lattice discretization and multirange potentials for the Shan–Chen model or MRT collision operator [21]. Another strategy to improve the gas–liquid ratio is to utilize different equations of state (EOS) of the pseudo-potential, i.e. Peng–Robinson EOS, Carnahan–Sterling EOS, etc. The spurious currents are suppressed, and a better gas–liquid ratio is achieved [23]. The present work uses the original Shan–Chen potential and this approach is valid for any given equation of state.

The MRT model was introduced by d'Humières [24] in 1992. The MRT collision operator is only 15% to 20% slower than the BGK collision operator [25], but it has many advantages in comparison with the BGK. These advantages include better stability [26] for performing low viscous fluid flow [27], ability to simulate phenomena with Prandtl number different from unity [25], and to improve effective location of simple boundaries [28] and interfaces [29]. The MRT has also been applied to simulate multiphase phenomena, e.g., Poiseuille flow in inclined channels with different kinematic viscosities [30] and for free-interface flow [14]. Tölke et al. [31] applied MRT for multiphase flow simulations on adaptive grids. McCracken et al. [32] incorporated the Carnahan–Sterling EOS into the force term. Later on, Abraham and Mukherjee [33] incorporated a pressure-based MRT high-density-ratio two-phase LBM, and claimed the ability to simulate density ratios up to 1000.

The MRT approaches were applied to the color multiphase model [5], free energy models, and the He multiphase model [7]. This research is a continuation for our previous work [21] with the MRT model applied to the Shan–Chen multiphase flow model and incorporates the multirange potential and extended equilibrium. The incorporation of the multirange potential gives the ability to include the correct Navier–Stokes surface tension term. The extended equilibrium improves the gas–liquid ratio for droplet simulations by 30%, and the MRT collision operator improves gas–liquid ratio by almost 30%. Thus, the combination of the MRT and the extended equilibria allows droplets with a gas–liquid density ratio up to 160%. In comparison with the BGK model, which allows droplets with a gas–liquid density ratio up to 100. We performed only Laplace test simulations for the droplet. However, dynamic tests will be considered in the future.

The paper is organized as follows. First, we give a brief introduction to the LBM theory. Second, we adopt the Shan–Chen model with MRT collision operator. The results of numerical experiments are then presented and discussed. Finally, the main findings and suggestions for further work are summarized.

### 1.1. Lattice Boltzmann equation

The Lattice Boltzmann Equation (LBE) with BGK [34] collision operator can be expressed as [35],

$$f_i(\boldsymbol{r} + \boldsymbol{c}_i \Delta t, t) - f_i(\boldsymbol{r}, t) = -\frac{f_i(\boldsymbol{r}, t) - f_i^{eq}(\boldsymbol{r}, t)}{\tau} \Delta t, \quad i = 0, \ldots, n-1. \tag{1}$$

For two-dimensional $n = 9$ velocities, kinematic viscosity of a fluid can be related to relaxation time as $\nu = \frac{1}{3}(\tau - \Delta t/2)$, where $\Delta t$ is the discretization time step. The equilibrium function has the following form:

$$f_i^{eq} = t_i \rho \left( c_s^2 + u_\alpha c_{i\alpha} + 3 \frac{Q_{i\alpha\beta} u_\alpha u_\beta}{2} \right), \tag{2}$$

where $\rho = \sum_i f_i$ and $\rho \boldsymbol{u} = \sum_i f_i \boldsymbol{c}_i$. The weights, $t_i$, are defined as follows

$$t_i = \begin{cases} 4/3, & \text{if } i = 0\,, \\ 1/3, & \text{if } i = 1, \ldots, 4\,, \\ 1/12, & \text{if } i = 5, \ldots, 9\,, \end{cases} \tag{3}$$

and $Q_{i\alpha\beta}$ is defined as

$$Q_{i\alpha\beta} = c_{i\alpha}c_{i\beta} - \frac{1}{3}\delta_{\alpha\beta}. \tag{4}$$

The left-hand side of Eq. (1) is the so-called streaming operator. The right-hand side of Eq. (1) is a collision operator. The streaming operator governs particle motion along the lattice directions $\boldsymbol{c}_i$. For the D2Q9 model the discrete velocities are

$$\begin{array}{lll} \boldsymbol{c}_0 = (0,0) & \boldsymbol{c}_1 = (1,0) & \boldsymbol{c}_2 = (0,1) \\ \boldsymbol{c}_3 = (-1,0) & \boldsymbol{c}_4 = (0,-1) & \boldsymbol{c}_5 = (1,1) \\ \boldsymbol{c}_6 = (-1,1) & \boldsymbol{c}_7 = (-1,-1) & \boldsymbol{c}_8 = (1,-1). \end{array}$$

The LBE is able to simulate a vast array of physical phenomena, including multiphase physics through incorporation of force. The next section describes the Shan–Chen approach for multiphase flows.

## 2. Shan–Chen model

In the Shan–Chen model [11], the surface tension term and equation of state is added to the LBM as an external force. In addition, the external force at a given node depends on all local neighbor characteristics located at the distance $\boldsymbol{c}_i$ from the node. Shan and Chen [11] introduced a pseudo-potential $\psi$ in the force. Pseudo-potential explicitly depends on density:

$$\boldsymbol{F} = G_1\psi(\boldsymbol{x})\sum_i t_i\psi(\boldsymbol{x}+\boldsymbol{c}_i)\boldsymbol{c}_i, \tag{5}$$

where $\boldsymbol{F}$ is the force in the Navier–Stokes equation, $G_1$ is the parameter controlling a gas–liquid ratio and surface tension. Typically, the Shan–Chen pseudo-potential is taken as $\psi = 1 - \exp(-\rho)$. The external force can be incorporated in many different ways. Ref. [36] describes strategies to incorporate the force term to the LBE with the BGK collision operator. This work adopts the original method of Shan and Chen for shifting velocity:

$$\rho\boldsymbol{u}' = \sum_i f_i\boldsymbol{c}_i + \boldsymbol{F}\tau. \tag{6}$$

This is easily incorporated with the MRT collision operator and improves the gas–liquid ratio. Such an inclusion of force [22] restores the Navier–Stokes equation with the macroscopic velocity:

$$\rho\boldsymbol{u}_{macro} = \sum_i f_i\boldsymbol{c}_i + \frac{\boldsymbol{F}}{2}. \tag{7}$$

### 2.1. Taylor expansion

The equation of state for the original LBE is given by [2]:

$$P = c_s^2\rho. \tag{8}$$

However, the inclusion of a density-dependent force term brings about a non-ideal contribution. The Shan–Chen force term for D2Q9, Eq. (5), can be expanded using a Taylor series expansion:

$$\begin{aligned} \boldsymbol{F} = {} & G_1\psi(x,y)(w_1\psi(x+c\Delta t,y)\boldsymbol{c}_1 + w_2\psi(x,y+c\Delta t)\boldsymbol{c}_2 + w_3\psi(x-c\Delta t,y)\boldsymbol{c}_3 + w_4\psi(x,y-c\Delta t)\boldsymbol{c}_4 \\ & + w_5\psi(x+c\Delta t,y+c\Delta t)\boldsymbol{c}_5 + w_6\psi(x-c\Delta t,y+c\Delta t)\boldsymbol{c}_6 + w_7\psi(x-c\Delta t,y-c\Delta t)\boldsymbol{c}_7 \\ & + w_8\psi(x+c\Delta t,y-c\Delta t)\boldsymbol{c}_8) = G_1\psi\left(\frac{1}{3}\nabla\psi + \frac{1}{18}\nabla\Delta\psi\right), \end{aligned} \tag{9}$$

where $\Delta t = 1$ is the time step, and $\Delta\psi$ represents the Laplacian operator $(\nabla\cdot\nabla)\psi$. Eq. (9) contains the equation of state term and the surface tension term.

### 2.2. Surface tension

The surface tension in Eq. (9) is represented as

$$\boldsymbol{F}_s = \frac{G_1}{18}\nabla\Delta\psi. \tag{10}$$

However, it is different from the proper surface tension presented by [32],

$$\boldsymbol{F}_s = k\nabla\Delta\rho. \tag{11}$$

Despite the fact that the Shan–Chen surface tension term, Eq. (10), is proportional to the usual surface tension term, Eq. (11) [18], many authors considered it a drawback. Note that surface tension and the equation of state depend on the same parameter $G_1$, which is a limitation of the Shan–Chen model.

After some algebra, the force term has the gradient for the force potential and non-gradient parts for the surface tension, as

$$\begin{aligned} F_\alpha &= G_1\psi\left(\frac{1}{3}\partial_\alpha\psi + \frac{1}{18}\partial_\alpha\Delta\psi\right) = G_1\left(\frac{1}{6}\partial_\alpha\psi^2 + \frac{1}{18}(\partial_\alpha(\psi\Delta\psi) - \Delta\psi\,\partial_\alpha\psi)\right) \\ &= G_1\left(\frac{1}{6}\partial_\alpha\psi^2 + \frac{1}{18}(\partial_\alpha(\psi\Delta\psi) + \frac{1}{2}\partial_\alpha(\nabla\psi)^2 - \partial_\beta\partial_\alpha\psi\,\partial_\beta\psi)\right). \end{aligned} \tag{12}$$

The momentum-flux tensor obeys a conservation equation [18]:

$$\partial_\beta\mathbb{P}_{\alpha\beta} = -F_\alpha + \partial_\alpha(p) = -F_\alpha + \partial_\alpha(c_s^2\rho).$$

Thus, the flux tensor $\mathbb{P}_{\alpha\beta}$ is modified due to the Shan–Chen force as follows:

$$\mathbb{P}_{\alpha\beta} = \left(c_s^2\rho + \frac{G_1}{6}\psi^2 + \frac{G_1}{18}|\nabla\psi|^2 + \frac{G_1}{6}\psi\Delta\psi\right)\delta_{\alpha\beta} - \frac{G_1}{18}\partial_\alpha\psi\,\partial_\beta\psi.$$

Surface tension is defined as the integral along a flat surface of the mismatch between the normal ($\mathbb{P}_{yy}$) and transversal ($\mathbb{P}_{xx}$) components of the flux tensor [18]:

$$\sigma = \int_{-\infty}^{+\infty}(\mathbb{P}_{yy} - \mathbb{P}_{xx})\mathrm{d}y = -\frac{G_1}{18}\int_{-\infty}^{+\infty}|\partial_y\psi|^2\mathrm{d}y.$$

The potential is given by

$$V = \frac{G_1}{6}\psi^2 + \frac{G_1}{18}|\nabla\psi|^2 + \frac{G_1}{18}\psi\Delta\psi. \tag{13}$$

However, the terms $\frac{G_1}{18}|\nabla\psi|^2$ and $\frac{G_1}{18}\psi\Delta\psi$ in Eq. (13) come from the surface tension term and therefore are not involved in the bulk equation of state:

$$p = c_s^2\rho + \frac{G_1}{6}\psi^2. \tag{14}$$

### 2.3. Multirange potential

There are different extensions of the Shan–Chen model. One such extension is to use the multirange potential. Succi et al. [18] suggested the multirange potential for the Shan–Chen multiphase model as:

$$\boldsymbol{F} = G_1\psi(\boldsymbol{r})\sum_i \psi(\boldsymbol{r} + \boldsymbol{c}_i\Delta t)\boldsymbol{c}_i + G_2\psi(\boldsymbol{r})\sum_i \psi(\boldsymbol{r} + 2\boldsymbol{c}_i\Delta t)\boldsymbol{c}_i. \tag{15}$$

By the Taylor series expansion, the following formula is obtained:

$$F_\alpha = \frac{G_1 + 2G_2}{3}\psi\,\partial_\alpha\psi + \frac{G_1 + 8G_2}{6}\psi\,\partial_\alpha\Delta\psi. \tag{16}$$

Notice that by taking $G_2 = -G_1/8$, the surface tension force term equals zero and the proper surface tension term, as stated in Eq. (11), is restored. Therefore, equating $G_2 = -G_1/8$ also allows the proper equation of state to be obtained by multiplying the force by 4/3:

$$\begin{aligned} F_\alpha &= \frac{4}{3}(F_1 + F_2) = \frac{4}{3}\frac{G_1 + 2G_2}{3}\psi\,\partial_\alpha\psi \\ &= \frac{G_1}{3}\psi\,\partial_\alpha\psi, \end{aligned}$$

which refers to the equation of state $p = c_s^2\rho + \frac{G_1}{6}\psi^2$ without any additional terms from surface tension.

### 2.4. Surface tension term discretization

Once the potential for the equation of state is known, the force term can be split into two parts. One part is related to the potential, and the other is related to the surface tension:

$$\boldsymbol{F} = \boldsymbol{F}_{pot} + \boldsymbol{F}_s, \tag{17}$$

where $\boldsymbol{F}_s = \frac{G_1}{18}\psi\nabla\Delta\psi$ according to the Shan–Chen formulation. This term will be replaced by $\boldsymbol{F}_s = k\rho\nabla\Delta\rho$. When using the extended multirange potential, the surface tension term will be discretized through a 25-point stencil discretization scheme. The treatment of the boundaries is beyond the scope of this paper, and will be addressed in future research.

Different numerical schemes may be used for discretization of the Laplacian or the gradient. Let us represent the stencil through the matrix below, where every element applies to the corresponding point in the lattice. Any 25-point stencil has the following form:

$$\begin{pmatrix} a_{11} & a_{12} & a_{13} & a_{14} & a_{15} \\ a_{21} & a_{22} & a_{23} & a_{24} & a_{25} \\ a_{31} & a_{32} & a_{33} & a_{34} & a_{35} \\ a_{41} & a_{42} & a_{43} & a_{44} & a_{45} \\ a_{51} & a_{52} & a_{53} & a_{54} & a_{55} \end{pmatrix}. \tag{18}$$

For the gradient of the Laplacian in the $x$-direction ($\partial_x\Delta$) some conditions are applied. First of all, it is asymmetric in the $x$-direction and symmetric in the $y$-direction:

$$\begin{pmatrix} a_{11} & a_{12} & 0 & -a_{12} & -a_{11} \\ a_{21} & a_{22} & 0 & -a_{22} & -a_{21} \\ a_{31} & a_{32} & 0 & -a_{32} & -a_{31} \\ a_{21} & a_{22} & 0 & -a_{22} & -a_{21} \\ a_{11} & a_{12} & 0 & -a_{12} & -a_{11} \end{pmatrix}. \tag{19}$$

After expanding, using Taylor series about the central point, the following equations are obtained:

$$\begin{aligned} &8a_{11} + 4a_{12} + 8a_{21} + 4a_{22} + 4a_{31} + 2a_{32} = 0 \\ &-16a_{11} - 8a_{12} - 4a_{21} - 2a_{22} = -\frac{16}{3}a_{11} - \frac{2}{3}a_{12} - \frac{16}{3}a_{21} - \frac{2}{3}a_{22} - \frac{8}{3}a_{31} - \frac{1}{3}a_{32}. \end{aligned} \tag{20}$$

The solution which we used in our calculations has the following form:

$$\partial_x\Delta = \frac{1}{72}\begin{pmatrix} -1 & -4 & 0 & 4 & 1 \\ -8 & 4 & 0 & -4 & 8 \\ -18 & 72 & 0 & -72 & 18 \\ -8 & 4 & 0 & -4 & 8 \\ -1 & -4 & 0 & 4 & 1 \end{pmatrix}. \tag{21}$$

Hence, the multirange force can be presented by a 25-point stencil, required for obtaining the surface tension term. However, for the gradient of the equation of state force potential:

$$\boldsymbol{F} = \frac{4}{3}(\boldsymbol{F}_1 + \boldsymbol{F}_2) = \frac{G_1}{6}\nabla\psi^2. \tag{22}$$

This requires only a 16-point stencil scheme. Every force $\boldsymbol{F}_1$ and $\boldsymbol{F}_2$ in Eq. (22) is presented with an 8-point stencil scheme, giving an overall 16-point stencil numerical scheme. The advantage of using the multirange potential is in obtaining a pure potential of the equation of state without additional surface tension terms. Then, the bulk equation of state without a surface tension term can be obtained, and one can add a proper surface tension term $k\rho\nabla\Delta\rho$ using the numerical stencil presented in Eq. (21).

Concluding this section, $G_2 = -G_1/8$ and the potential force was taken as:

$$\boldsymbol{F}_{pot} = \frac{4}{3}(\boldsymbol{F}_1 + \boldsymbol{F}_2) = \frac{4}{3}\left(G_1\psi(\boldsymbol{r})\sum_i \psi(\boldsymbol{r} + \boldsymbol{c}_i)\boldsymbol{c}_i + G_2\psi(\boldsymbol{r})\sum_i \psi(\boldsymbol{r} + 2\boldsymbol{c}_i)\boldsymbol{c}_i\right). \tag{23}$$

## 3. Matrix representation

There are several possible ways to represent the collision operator. They include the BGK with single-relaxation time [35], the TRT with two-relaxation time [37], and the MRT with multiple-relaxation times [24,26,32,38] following the original idea of Higuera et al. [39].

In general, one possible series expansion of the matrix collision operator is formulated as [20]:

$$\Omega f^{neq} = \int \Omega(\boldsymbol{v}, \boldsymbol{v}', \boldsymbol{r}, t)(f^{eq}(\boldsymbol{v}') - f(\boldsymbol{v}))\mathrm{d}\boldsymbol{v}',$$

where

$$\Omega(\boldsymbol{v}, \boldsymbol{v}', \boldsymbol{r}, t) = W(v)\sum_k H_k(\boldsymbol{v})w_k(\boldsymbol{r}, t)H_k(\boldsymbol{v}'),$$

where $H_k$ is the Hermite polynomial of $k$th order. Let us reformulate the collision operator as in [39]:

$$\Omega f^{neq} = \sum_j A_{ij}(f_j^{eq} - f_j).$$

Thus, the Lattice Boltzmann Equation takes the form:

$$f_i(\boldsymbol{r} + \boldsymbol{c}_i\Delta t, t) - f_i(\boldsymbol{r}, t) = -\sum_j A_{ij}(f_j(\boldsymbol{r}, t) - f_j^{eq}(\boldsymbol{r}, t)). \tag{24}$$

The right-hand side of Eq. (24) contains the matrix $A_{ij}$, which can be analyzed in terms of eigenvalues and eigenvectors.

### 3.1. Matrix eigenvectors

The eigenvector basis used in this research was proposed by Benzi et al. [40], which can be obtained through the Hermite series of the collision operator [20]. In our study, we restrict this model to one free eigenvalue. The MRT D2Q9 model originated from the work of d'Humières [24] and was further studied in [26]. The model has two free eigenvalues for compressible flow and three free eigenvalues for incompressible flow, to control and eliminate expansion errors and stability limits. One variation of this model is the two-relaxation TRT model proposed by Ginzburg in [37].

The eigenvectors used are:

$$\begin{aligned}
|A_\rho\rangle &= (1, 1, 1, 1, 1, 1, 1, 1, 1)/\sqrt{3},\\
|A_{J_x}\rangle &= (0, 1, 0, -1, 0, 1, -1, -1, 1),\\
|A_{J_y}\rangle &= (0, 0, 1, 0, -1, 1, 1, -1, -1),\\
|A_{\mathbb{P}_{xx}}\rangle &= (-1/3, 2/3, -1/3, 2/3, -1/3, 2/3, 2/3, 2/3, 2/3)\sqrt{3}/\sqrt{2},\\
|A_{\mathbb{P}_{xy}}\rangle &= (0, 0, 0, 0, 0, 1, -1, 1, -1)\sqrt{3},\\
|A_{\mathbb{P}_{yy}}\rangle &= (-1/3, -1/3, 2/3, -1/3, 2/3, 2/3, 2/3, 2/3, 2/3)\sqrt{3}/\sqrt{2},\\
|A_{J_\gamma}\rangle &= (1, -2, -2, -2, -2, 4, 4, 4, 4)/\sqrt{12},\\
|A_{J_{\gamma x}}\rangle &= (0, -2, 0, 2, 0, 4, -4, -4, 4)\sqrt{2}/4,\\
|A_{J_{\gamma y}}\rangle &= (0, 0, -2, 0, 2, 4, 4, -4, -4)\sqrt{2}/4.
\end{aligned}$$

The eigenvectors corresponding to the equilibrium moments of the Navier–Stokes equation can be written as [38],

$$|\rho, J_x, J_y, \mathbb{P}_{xx}, \mathbb{P}_{xy}, \mathbb{P}_{yy}, J_\gamma, J_{\gamma x}, J_{\gamma y}\rangle = \rho|1, u_x, u_y, u_x^2, u_xu_y, u_y^2, u_x^2u_y^2, u_xu_y^2, u_yu_x^2\rangle. \tag{25}$$

The last three terms are needed to properly restore the pressure tensor through the Chapman–Enskog expansion, as stated in [20]. This matrix representation differs from the matrix presented in [25,26]. One can find the usage of this matrix representation in [39,38,21]. Notice that different representations do not affect the underlying physics. The eigenvectors choice is arbitrary in some subgroups taken from group theory [41] and may influence the analysis of eigenvalue problems.

The first six eigenvectors are needed to restore the Navier–Stokes equation with density, momentum conservation, and the proper viscous terms. The remaining three eigenvectors are identified through Hermite polynomials in the velocity space, which are orthogonal to all other six eigenvectors. The remaining eigenvalues are denoted by $\omega_6 = \gamma, \omega_7 = \gamma_x, \omega_8 = \gamma_y$. The eigenvalues $\gamma$, $\gamma_x$ and $\gamma_y$ can be tuned to improve the stability of LBM [26]. The three eigenvalues $\gamma$, $\gamma_x$ and $\gamma_y$ are called "ghost" eigenvalues, because they are needed for symmetry reasons, although they are not required for restoration of the Navier–Stokes equation [40].

### 3.2. Eigenvectors decomposition and momentum formulation

The collision matrix can be represented, as

$$A_{ij} = t_i \sum_k A_i^{(k)} \omega_k A_j^{(k)}, \tag{26}$$

where $t_i$ are the weights defined in Eq. (3), and $A^{(k)}$ are the eigenvectors given above.

The orthogonality conditions [21] are

$$\sum_k t_i A_i^{(k)} A_j^{(k)} = \delta_{ij},$$

$$\sum_i t_i A_i^{(j)} A_i^{(k)} = \delta_{jk}.$$

The moments of the LBM can be introduced as:

$$F_k = \sum_i f_i A_i^{(k)}, \tag{27}$$

where $F_k$ are the kinetic moments from Eq. (25). However, the inverse formula explicitly includes the weights:

$$f_i = t_i \sum_i F_k A_i^{(k)}. \tag{28}$$

### 3.3. Collision operator and force incorporation

The collision operator can be written in terms of eigenvectors, eigenvalues and kinetic moments:

$$\begin{aligned}\sum_j A_{ij}(f_j - f_j^{eq}) &= \sum_j (f_j - f_j^{eq}) t_i \sum_k A_i^{(k)} \omega_k A_j^{(k)} = \sum_k t_i A_i^{(k)} \omega_k \sum_j (f_j - f_j^{eq}) A_j^{(k)} = \sum_k t_i A_i^{(k)} \omega_k (F_k - F_k^{eq}) \\ &= t_i \big( \omega_0 1_i (\rho - \rho^{eq}) + \omega_1 c_{ix} (J_x - J_x^{eq}) + \omega_2 c_{iy} (J_y - J_y^{eq}) \\ &\quad + \omega_3 \mathbb{Q}_{ixx} (\mathbb{P}_{xx} - \mathbb{P}_{xx}^{eq}) + \omega_4 \mathbb{Q}_{ixy} (\mathbb{P}_{xy} - \mathbb{P}_{xy}^{eq}) + \omega_5 \mathbb{Q}_{iyy} (\mathbb{P}_{yy} - \mathbb{P}_{yy}^{eq}) \\ &\quad + \omega_6 g_i (J_\gamma - J_\gamma^{eq}) + \omega_7 g_i c_{ix} (J_{\gamma_x} - J_{\gamma_x}^{eq}) + \omega_8 g_i c_{iy} (J_{\gamma_y} - J_{\gamma_y}^{eq}) \big).\end{aligned} \tag{29}$$

For force incorporation the appropriate series of force due to eigenvectors of the matrix $A$ should be introduced:

$$S_i = t_i \sum_k s_k A_i^k = t_i \big( s_0 1_i + s_1 c_{ix} + s_2 c_{iy} + s_3 \mathbb{Q}_{ixx} + + s_4 \mathbb{Q}_{ixy} + s_5 \mathbb{Q}_{iyy} + s_6 g_i + s_7 g_i c_{ix} + s_8 g_i c_{iy} \big),$$

where $s_k$ are moments of the force. To be consistent with the restoration of the force term in the Navier–Stokes equation, the above expression becomes:

$$S_i = t_i \left( F_{i\alpha} c_{i\alpha} + 3\rho \frac{F_\alpha u_\beta + F_\beta u_\alpha}{2} \left[ c_{i\alpha} c_{i\beta} - \frac{1}{3} \delta_{\alpha\beta} \right] + s_6 g_i + s_7 g_{ix} + s_8 g_{iy} \right).$$

The interested reader can find all details about force incorporated in [21].

In the current investigation, we are interested when all eigenvalues are non-zero. This imposes a new equilibrium distribution function $\tilde{f}^{eq}$, defined as:

$$\tilde{f}_i^{eq} = t_i \left( c_s^2 + c_{i\alpha} \left( u_\alpha + \frac{F_\alpha}{\omega_\alpha} \right) + \frac{3}{2} \mathbb{Q}_{i\alpha\beta} \left( u_\alpha - \frac{F_\alpha}{\omega_{\alpha\beta}} \right) \left( u_\beta - \frac{F_\beta}{\omega_{\alpha\beta}} \right) + \tilde{s}_6 g_i + \tilde{s}_7 g_i c_{ix} + \tilde{s}_8 c_{iy} \right), \tag{30}$$

where $\omega_\alpha = \omega_{1,2}, \omega_{\alpha\beta} = \omega_{3,4,5}, \tilde{s}_{6,7,8} = s_{6,7,8} + J_{\gamma_{x,y}}^{eq}$. Notice that we have a few additional degrees of freedom when tuning $w_{6,7,8}$. By tuning the ghost eigenvalues, one can improve stability [26,21].

### 3.4. Truncated and extended equilibria

The usual choice for BGK-based simulations of the Shan–Chen force when equilibrium distribution function contains terms up to the 2nd moment of the Navier–Stokes equation is:

$$f_i^{eq} = t_i \rho \left( c_s^2 + u_\alpha c_{i\alpha} + 3 \frac{\mathbb{Q}_{i\alpha\beta}}{2} u_\alpha u_\beta \right), \tag{31}$$

where velocity is shifted due to the force $\rho \boldsymbol{u} = \sum_i f_i \boldsymbol{c}_i + \boldsymbol{F}\tau$. One can check that this implies ghost equilibrium moments equal to 0, i.e. $\sum f_i^{eq} A_{\gamma_i} = 0$. Also, by setting ghost eigenvalues to 0, new conservation laws appear. The great majority of MRT models set non-zero conditions for ghost eigenvalues and ghost moments. Here, the extended equilibrium moments imply non-zero ghost moments, such as $J_\gamma = \rho u_x^2 u_y^2, J_{\gamma_y} = \rho u_x^2 u_y J_{\gamma_x} = \rho u_x u_y^2$.

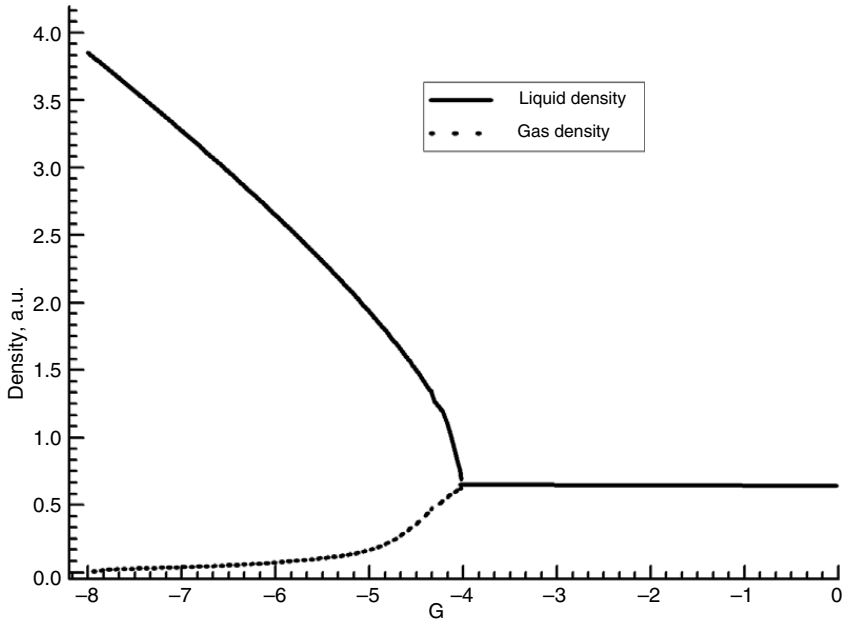


**Fig. 1.** Gas and liquid density dependence on $G_1$. There is no separation until $G_1$ equals $G_{crit} = -4$. The initial density was taken as $\rho = \rho_{crit} = \ln 2$.

### 3.5. Equilibrium moments

The eigenvectors corresponding to the moments of the Navier–Stokes equation can be written as [38]:

$$|\rho, J_x, J_y, \mathbb{P}_{xx}, \mathbb{P}_{xy}, \mathbb{P}_{yy}, J_\gamma, J_{\gamma x}, J_{\gamma y}\rangle = \rho|1, u_x, u_y, u_x^2, u_x u_y, u_y^2, u_x^2 u_y^2, u_x u_y^2, u_y u_x^2\rangle. \tag{32}$$

They can be obtained through a Hermite expansion of the equilibrium distribution function [20]. Thus, the enhanced equilibrium distribution function will be:

$$f_i^{eq} = \rho t_i \left( c_s^2 + c_{i\alpha} u_\alpha + 3\frac{\mathbb{Q}_{i\alpha\beta} u_\alpha u_\beta}{2} + \frac{g_i}{12} u_x^2 u_y^2 + \frac{g_i c_{ix}}{8} u_x u_y^2 + \frac{g_i c_{iy}}{8} u_x^2 u_y \right), \tag{33}$$

where

$$\rho u_\alpha = \sum_i f_i c_{i\alpha} + \frac{F_\alpha}{\omega_{1\div 8}}. \tag{34}$$

There are ghost moments of force, namely $s_{6,7,8}$, in Eq. (30). Following the approach for BGK force incorporation, we allow higher-order force terms $s_{6,7,8}$ to have shifting velocity terms.

## 4. Numerical results

### 4.1. Problem statement

Increasing $|G_1|$ in the Shan–Chen force, Eq. (5), results in the increase of the gas–liquid ratio to be simulated. One can obtain the gas–liquid density from the equation of state, Eq. (14), shown in Fig. 1.

There is a point on a $G_1$ curve where the simulation blows up. It is stated in [18] that this occurs due to the anisotropic higher-order force terms coming from Taylor series expansion.

To illustrate the superiority of the described model, a square domain with periodical boundary conditions sized $128 \times 128$ nodes was considered. Liquid droplets with 20 units radii are put in the center of the domain for 2000 time-steps. The initial gas and liquid density are taken from the equation of state for a fixed $G_1$ value. We take $\omega_{0\div 5} = 1$ and only tune $\omega_{6\div 8}$.

### 4.2. Results

#### 4.2.1. Gas–liquid density ratio

To illustrate the superiority of the model presented we examined the following initial conditions and numerical schemes:

(1) When examining the droplet, the steady-state condition has small relative velocities and the influence of the second-order velocity term in the equilibrium distribution function is questionable. We simulated the droplet initialized with

the density values from the equation of state (with or without the multirange potential) and Stokes equilibrium, given below:

$$f_i^{eq} = t_i\rho\left(c_s^2 + u_\alpha c_{i\alpha}\right), \tag{35}$$

where $\rho u_\alpha = \sum_i f_i c_{i\alpha} + F/\omega_{x,y}$.

Stokes equilibrium yields positive densities until $G_1 = -6.2$, which corresponds to a liquid density of 2.73 and a gas density of 0.102. This gives a gas–liquid density ratio of 26.7. Increase of $|G_1|$ is stable, but the densities become negative, so the gas branch on large $G_1$ does not correspond to the equation of state.

(2) Navier–Stokes equilibrium, Eq. (2), with BGK collision operator without the multirange potential with forcing included in the linear term as $\rho\hat{u}_\alpha = \sum_i f_i c_{i\alpha} + F/\omega$ and in the non-linear second-order term as $\rho\tilde{u}_\alpha = \sum_i f_i c_{i\alpha} + F/2$ without fourth- and third-order polynomials in the equilibrium, can be presented as:

$$f_i^{eq} = t_i\rho\left(c_s^2 + \hat{u}_\alpha c_{i\alpha} + 3\frac{Q_{i\alpha\beta}\tilde{u}_\alpha\tilde{u}_\beta}{2}\right). \tag{36}$$

The scheme does not "fail" until $G_1 = -5.2$ with a gas density of 0.0936 and a liquid density of 2.0582, corresponding to a gas–liquid density ratio of 22.

(3) Navier–Stokes equilibrium, Eq. (2), with the BGK collision operator without the multirange potential with shifting velocity in linear and non-linear terms without fourth- and third-order polynomials in the equilibrium, can be presented as:

$$f_i^{eq} = t_i\rho\left(c_s^2 + \tilde{u}_\alpha c_{i\alpha} + 3\frac{Q_{i\alpha\beta}\tilde{u}_\alpha\tilde{u}_\beta}{2}\right), \tag{37}$$

where $\rho\tilde{u}_\alpha = \sum_i f_i c_{i\alpha} + F/\omega_{1\div 8}$. As discussed earlier for the BGK we take $\omega_{1\div 8} = 1$. The scheme is stable until $G_1 = -8.2$, which corresponds to a gas–liquid ratio of 100.

(4) Navier–Stokes equilibrium, Eq. (2), with BGK collision operator without the multirange potential with forcing included in the linear term as $\rho\hat{u}_\alpha = \sum_i f_i c_{i\alpha} + F/\omega$ and in the non-linear second-order terms as $\rho\tilde{u}_\alpha = \sum_i f_i c_{i\alpha} + F/2$ with fourth- and third-order polynomials in the equilibrium, can be presented as:

$$f_i^{eq} = t_i\rho\left(c_s^2 + \hat{u}_\alpha c_{i\alpha} + 3\frac{Q_{i\alpha\beta}\tilde{u}_\alpha\tilde{u}_\beta}{2} + \frac{g_i}{12}\tilde{u}_x^2\tilde{u}_y^2 + \frac{g_i c_{ix}}{8}\tilde{u}_x\tilde{u}_y^2 + \frac{g_i c_{iy}}{8}\tilde{u}_x^2\tilde{u}_y\right). \tag{38}$$

In this case the addition of a third- and fourth-order polynomial does not improve the scheme. Nonetheless, the scheme is stable until $G_1 = -5.2$.

(5) Navier–Stokes equilibrium, Eq. (2), with MRT collision operator without the multirange potential with shifting velocity in linear and non-linear terms with fourth- and third-order polynomials in the equilibrium can be presented as:

$$f_i^{eq} = t_i\rho\left(c_s^2 + \tilde{u}_\alpha c_{i\alpha} + 3\frac{Q_{i\alpha\beta}\tilde{u}_\alpha\tilde{u}_\beta}{2} + \frac{g_i}{12}\tilde{u}_x^2\tilde{u}_y^2 + \frac{g_i c_{ix}}{8}\tilde{u}_x\tilde{u}_y^2 + \frac{g_i c_{iy}}{8}\tilde{u}_x^2\tilde{u}_y\right) \tag{39}$$

where $\rho\tilde{u}_\alpha = \sum_i f_i c_{i\alpha} + F/\omega_{1\div 8}$. The scheme is stable until $G_1 = -8.5$ with a gas density of 0.0374 and a liquid density of 4.2165 corresponding to a gas–liquid density ratio of 112.

(6) The same as case (3) with the multirange potential gives the stable regime until $G_1 = -8.5$ with a gas density of 0.0374 and a liquid density of 4.2204, corresponding to a gas–liquid density ratio of 118.

(7) The same as case (5) with the multirange potential results in the stable regime until $G_1 = -8.7$ with a gas density of 0.0329 and a liquid density of 4.3271, corresponding to a gas–liquid density ratio of 132.

(8) This simulation involved the proper tuning of ghost eigenvalues ($\omega_{5\div 8} = \omega_{\gamma,\gamma_x,\gamma_y} = 0.75$). The model is stable until $G_1 = -8.85$ with a gas density 0.0275 and a liquid density of 4.4089, which corresponds to a gas–liquid density ratio of 160.

#### 4.2.2. Laplace–Young test

To illustrate that the modified model properly simulates multiphase physics, we performed the Laplace–Young test. The results are in Fig. 2. The Laplace–Young test states that the bulk pressure $p_{bulk} = c_s^2\rho + \frac{G_1}{6}\psi^2(\rho)$ difference between gas and liquid should be proportional to the surface tension term and inversely proportional to the droplet radius.

#### 4.2.3. Interface profiles

By introducing a surface tension coefficient $k$, we can simulate interface thickness with the fixed gas–liquid ratio. The main difference between the presented model and the generalized model [18] is that the interface thickness is controlled by a proper surface tension. This term is proportional to $\rho\nabla\Delta\rho$. This contrasts with the original model, where it is proportional to $\psi\nabla\Delta\psi$. Fig. 3 presents examples of varying interface thickness.

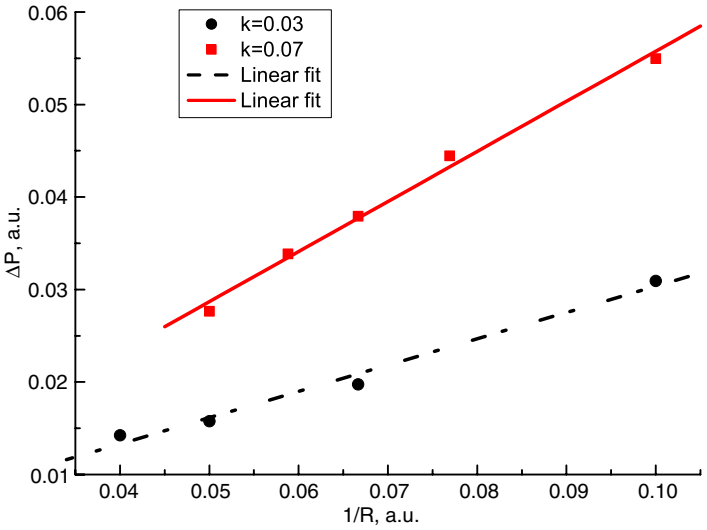


**Fig. 2.** Laplace test with modified equilibrium distribution function and tuned ghost eigenvalues.

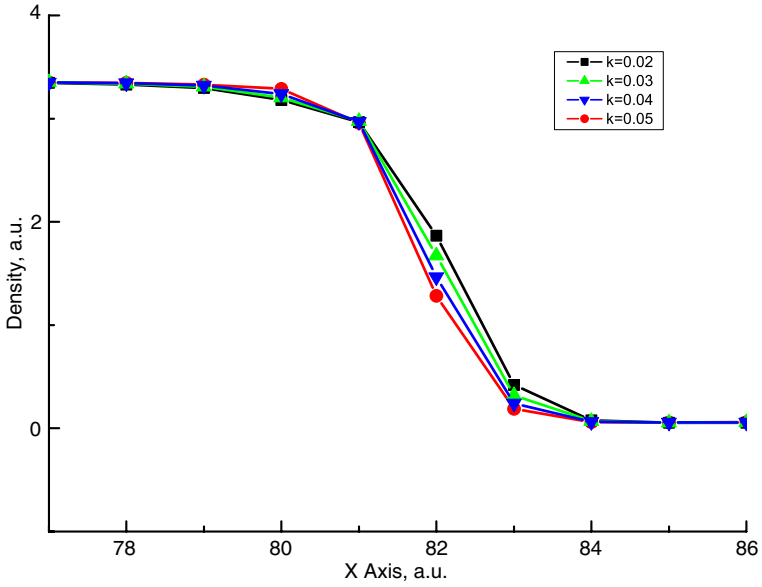


**Fig. 3.** Density profiles for different surface tension coefficients $k$.

## 5. Conclusion

The proposed model combines the multirange Shan–Chen force with a discretized surface tension and matrix collision operator, with an expanded equilibrium distribution function. Though a theoretical basis is not yet established, numerical simulations show that the stability limit and gas–liquid density ratio are improved. The model allows the proper inclusion of the Navier–Stokes surface tension term. This allowed the simulation of the gas–liquid density ratio up to 160. The model should work in the three-dimensional case, though the application test for it is a task for the future.

## Acknowledgments

A. Kuzmin would like to thank Alberta Ingenuity Fund for their financial support. The authors are grateful to Dr. I. Ginzburg for her insightful comments on this paper.

## References

[1] D. Yu, R. Mei, L.-S. Luo, W. Shyy, Viscous flow computations with the method of lattice Boltzmann equation, Prog. Aerosp. Sci. 39 (2003) 329–367.
[2] S. Succi, The Lattice Boltzmann Equation for Fluid Dynamics and Beyond, Oxford University Press, Oxford, 2001.
[3] M.C. Sukop, D.T. Thorne, Lattice Boltzmann Modeling an Introduction for Geoscientists and Engineers, Springer-Verlag, Berlin, 2005.
[4] A.A. Mohamad, Applied lattice Boltzmann method for transport phenomena, momentum, Heat and Mass Transfer, Sure Print, Calgary, 2007.

[5] D.H. Rothman, J.M. Keller, Immiscible cellular-automaton fluids, J. Statist. Phys. 52 (3–4) (1988) 1119–1127.
[6] A.K. Gunstensen, D.H. Rothman, S. Zaleski, G. Zanetti, Lattice Boltzmann model of immiscible fluids, Phys. Rev. A 43 (8) (1991) 4320–4327.
[7] X. He, X. Shan, G.D. Doolen, Discrete Boltzmann equation model for nonideal gases, Phys. Rev. E 57 (1) (1998) 1–14.
[8] M.R. Swift, W.R. Osborn, J.M. Yeomans, Lattice Boltzmann Simulation of Nonideal Fluids, Phys. Rev. Lett. 75 (5) (1995) 831–834.
[9] L.-S. Luo, Unified theory of lattice Boltzmann models for non-ideal gases, Phys. Rev. Lett. 81 (8) (1998) 1618–1621.
[10] T. Lee, C.-L. Lin, Pressure evolution lattice-Boltzmann-equation method for two-phase flow with phase change, Phys. Rev. E 67 (056703) (2003) 1–10.
[11] X. Shan, H. Chen, Simulation of nonideal gases and gas–liquid phase transitions by the lattice Boltzmann Equation, Phys. Rev. E 49 (4) (1994) 2941–2948.
[12] R.R. Nourgaliev, T.N. Dinh, T.G. Theofanous, D. Joseph, The lattice Boltzmann equation method: Theoretical interpretation, numerics and implications, Int. J. Multiph. Flow 29 (2003) 117–169.
[13] B. Ahrenholz, J. Tölke, P. Lehmann, A. Peters, M. Krafczyk, W. Durner, Prediction of capillary hysteresis in a porous material using lattice-Boltzmann methods and comparison to experimental data and a morhphological pore network model, Adw. Water. Res. 31 (9) (2008) 1151–1173.
[14] I. Ginzburg, K. Steiner, A free-surface lattice Boltzmann method for modelling the filling of expanding cavities by Bingham fluids, Phil. Trans. R. Soc. Lond. A 360 (2002) 453–466.
[15] D. Kehrwald, Numerical analysis of immiscible lattice BGK, Ph.D. Thesis, Fraunhofer-Institut für Techno- und Wirtschaftsmathematik, 2002.
[16] J. Thömmes, J. Becker, M. Junk, A.K. Vaikuntam, D. Kerhwald, A. Klar, K. Steiner, A. Wiegmann, A lattice Boltzmann method for immiscible multiphase flow simulations using the level set method, Technical Report, Fraunhofer-Institut für Techno- und Wirtschaftsmathematik ITWM, 2007.
[17] A.J. Briant, A.J. Wagner, J.M. Yeomans, Lattice Boltzmann simulations of contact line motion. I. Liquid-gas systems, Phys. Rev. E 69 (031602) (2004) 1–14.
[18] M. Sbragaglia, R. Benzi, L. Biferali, S. Succi, K. Sugiyama, F. Toschi, Generalized lattice Boltzmann method with multirange potential, Phys. Rev. E 75 (026702) (2007) 1–13.
[19] M. Latva-Kokko, D.H. Rothman, Diffusion properties of gradient-based lattice Boltzmann models of immiscible fluids, Phys. Rev. E 71 (056702) (2005) 1–8.
[20] X. Shan, X.-F. Yuan, H. Chen, Kinetic theory representation of hydrodynamics: A way beyond the Navier-Stokes equation, J. Fluid Mech. 550 (2006) 413–441.
[21] A. Kuzmin, A.A. Mohamad, S. Succi, Multi relaxation time lattice Boltzmann model for multiphase flows, Internat. J. Modern Phys. C 19 (6) (2008) 875–902.
[22] X. Shan, Analysis and reduction of the spurious current in a class of multiphase lattice Boltzmann models, Phys. Rev. E 73 (047701) (2006) 1–4.
[23] P. Yuan, L. Schaefer, Equations of state in a lattice Boltzmann model, Phys. Fluids 18 (042101) (2006) 1–11.
[24] D. d'Humières, Generalized lattice-Boltzmann equations. Rarefied gas dynamics: Theory and simulations, Prog. Astronaut. Aeronaut. 159 (1992) 450–458.
[25] D. d'Humières, I. Ginzburg, M. Krafczyk, P. Lallemand, L.-S. Luo, Multiple-relaxation-time lattice Boltzmann models in three dimensions, Phil. Trans. R. Soc. Lond. 360 (2002) 437–451.
[26] P. Lallemand, L.-S. Luo, Theory of the lattice Boltzmann method: Dispersion, dissipation, isotropy, Galilean invariance, and stability, Phys. Rev. E 61 (6) (2000) 6546–6562.
[27] K.N. Premnath, J. Abraham, Three-dimensional multi-relaxation time (MRT) lattice-Boltzmann models for multiphase flow, J. Comput. Phys. 224 (2007) 539–559.
[28] I. Ginzburg, F. Verhaeghe, D. d'Humières, Two-relaxation-time lattice Boltzmann scheme: About parametrization, velocity, pressure and mixed boundary conditions, Commun. Comput. Phys. 3 (2008) 427–478.
[29] I. Ginzburg, Lattice Boltzmann modeling with discontinuous collision components. Hydrodynamic and advection-diffusion equations, J. Statist. Phys. 126 (2007) 157–203.
[30] I. Ginzbourg, P.M Adler, Surface tension models with different viscosities, Transp. Porous Media 20 (1995) 37–76.
[31] J. Tölke, S. Freudiger, M. Krafczyk, An adaptive scheme using hierarchical grids for lattice Boltzmann multi-phase flow simulations, Comput. Fluids 35 (2006) 820–830.
[32] M.E. McCracken, J. Abraham, Multiple-relaxation-time lattice-Boltzmann model for multiphase flow, Phys. Rev. E 71 (036701) (2005) 1–9.
[33] S. Mukherjee, J. Abraham, A pressure-evolution-based multi-relaxation-time high-density-ratio two-phase lattice-Boltzmann model, Comput. Fluids 36 (2007) 1149–1158.
[34] P.L. Bhatnagar, E.P. Gross, M. Krook, A model for collision processes in gases. I.Small amplitude processes in charged and neutral one-component systems, Phys. Rev. 94 (3) (1954) 511–525.
[35] Y.H. Qian, D. d'Humières, P. Lallemand, Lattice BGK models for Navier-Stokes equation, Europhys. Lett. 17 (6) (1992) 479–484.
[36] Z. Guo, C. Zheng, B. Shi, Discrete lattice effects on the forcing term in the lattice Boltzmann method, Phys. Rev. E 65 (046308) (2002) 1–6.
[37] I. Ginzburg, Equilibrium-type and link-type lattice Boltzmann models for generic advection and anisotropic-dispersion equation, Adv. Wat. Res. 28 (2005) 1171–1195.
[38] P. Asinari, Semi-implicit-linearized multiple-relaxation-time formulation of lattice Boltzmann schemes for mixture modeling, Phys. Rev. E 73 (2006) 1–24.
[39] F.J. Higuera, J. Jimenez, Boltzmann approach to lattice gas simulations, Europhys. Lett. 9 (7) (1989) 663–668.
[40] R. Benzi, S. Succi, M. Vergassola, The lattice Boltzmann equation: Theory and applications, Phys. Rep. 222 (3) (1992) 145–197.
[41] R. Rubinstein, L.-S. Luo, Theory of the lattice Boltzmann equation: Symmetry properties of discrete velocity sets, Phys. Rev. E 77 (036709) (2008) 1–11.